



# MHD FREE CONVECTION AND HEAT TRANSFER FLOW THROUGH A VERTICAL POROUS PLATE IN THE PRESENCE OF CHEMICAL REACTION

R. Biswas<sup>a</sup>, M. Afikuzzaman<sup>b\*</sup>, M. Mondal<sup>a</sup>, S.F. Ahmmed<sup>a</sup>

<sup>a</sup> *Mathematics Discipline, Science, Engineering and Technology School, Khulna University, Khulna-9208, Bangladesh.*

<sup>b</sup> *Department of Mechanical Engineering, University of Newcastle, NSW-2308, Australia*

## ABSTRACT

Present study concerns with the numerical investigation of the MHD free convection and heat transfer fluid flow through a semi-infinite vertical porous plate with the effects of chemical reaction. A boundary layer approximation is premeditated to develop a flow model representing time dependent momentum, energy and concentration equations. The governing model equations are governed as a form of coupled nonlinear dimensionless system of partial differential equations (PDEs) by the as usual mathematical procedure of mathematical transformation and which model equations are solved by using explicit finite difference method (EFDM). Then the numerical results have been calculated by Compaq Visual FORTRAN (CVF) 6.6a and the obtained results have been capitalized for the variations of various dimensionless parameters on velocity, temperature and concentration profiles along with the skin friction coefficient, Nusselt number, Sherwood number, Isotherms and Streamlines. At the end, the obtained results are plotted and discussed after stability convergence test (SCT) by the using graphics software tecplot-9. An increases in the Grashof number is to increase the velocity distributions but by increasing the magnetic parameter which reduces the velocity profiles whereas increasing the heat generation parameter which increase the temperature profile.

**Keywords:** *Free convection, chemical reaction, MHD, Porous medium.*

## 1. INTRODUCTION

Free convection is a mechanism or type of transport in which the fluid motion is not generated by any external source. It is associated with natural convection like, relativity law, heat coefficient etc. MHD free convection and mass transfer flow through a vertical oscillatory porous plate with Hall, ion-slip currents and heat source in a rotating system has been scrutinized by Hossain *et al.* (2015). Effect logs of double diffusion on MHD Prandtl nano fluid adjacent to 4 stretching surface by the way of numerical approach has been performed by Bilal *et al.* (2017). They have instituted about the characteristics of nanofluids by constructing formulation of Prandtl fluid model and the solution of governing dimensionless problem had been executed by shooting method. Khalid *et al.* (2015) have reported the unsteady MHD free convection flow of Casson fluid past over an oscillating vertical plate embedded in a porous medium. Also, the unsteady Casson nanofluid flow over a stretching sheet with thermal radiation, convective and slip boundary conditions has been constructed by Oyelakin *et al.* (2016). Study of nanofluid flow and heat transfer between non-parallel stretching walls considering Brownian motion has been studied by Dogonchi *et al.* (2016). Also, Ramesh *et al.* (2016) have scrutinized the stagnation point flow of Maxwell fluid towards a permeable surface in the presence of nanoparticles.

Now a days, the study of chemical reaction is a process that leads to the transformation of one set of chemical substances to another. Classically, chemical reactions encompass changes that only involve the positions of electrons in the forming and breaking of chemical bonds between atoms with no change to the nuclei. Nuclear chemistry is a sub-discipline of chemistry that involves the chemical reactions of unstable and radioactive elements where both electronic and nuclear changes can occur. Chemical reactions happen at a characteristic reaction rate at a

given temperature and chemical concentration. During such chemical reactions, there is always generating of heat. The most common fluid fluids like water and air are contaminated with impurities like  $CO_2$ ,  $C_6H_6$  and  $H_2SO_4$  etc. Chemical reaction parameter shows a retarding effect on concentration distribution as the reaction proceeds from constructive to destructive state. Seth *et al.* (2014) have elaborated the effects of Hall current, radiation and rotation on natural convection heat and mass transfer flow past a moving vertical plate. Nonlocal vibration of y-shaped CNT conveying nano-magnetic viscous fluid under magnetic field has been examined by Arni *et al.* (2015). Characterization of chemical reaction on heat transfer through the nanofluid has been discussed by Das *et al.* (2016).

The effect of heat generation on boundary layer fluid flow is very significant due to engineering applications such as fire and combustion, metal waste, radioactive materials, reactor safety analysis, spent nuclear fuel etc. The heat transfer in convective mode is divided into two basic processes. If no externally induced flow is provided and flow arises naturally simply owing to the effect of a density difference, resulting from a temperature or concentration difference in a body force field, such as the gravitational field, the process is referred to the natural convection. On the other hand if the motion of the fluid is caused by an external agent such as the externally imposed flow of a fluid stream over a heated object, the process is termed as force convection. In the force convection, the fluid flow is generated by an external source such as a fan, a blower and the wind or the motion of the heated object itself. Such problems are very frequently encountered in technology where the heat transfers to or from a body is often due to an imposed flow of a fluid at a different temperature from that of a body. On the other side, in the natural convection, the density difference gives rise to buoyancy effects, owing to which the flow is generated. A heated body cooling in ambient air generates such a flow in the region surrounding it.

Similarly the buoyant flow arising from heat rejection to the atmosphere and to other ambient media, circulations arising in heated rooms, in the atmosphere, and in bodies of water, rise of buoyant flow to cause thermal stratification of the medium, as in temperature inversion and many other such heat transfer process in our natural environment, as well as in many technological applications, are included in the area of natural convection. The flow may also arise owing to concentration differences such as those caused by salinity differences in the sea and by composition differences in chemical processing unit, and these cause a natural convection mass transfer. Characterization of chemical reaction on heat transfer through the nanofluid has been introduced by Srikantha *et al.* (2015). Mahanta *et al.* (2016) have introduced the 3D Casson fluid flow past a porous linearly stretching sheet with convective boundary condition. Ahmed *et al.* (2017) have explored about the effects on magnetic field in squeezing flow of a Casson fluid between parallel plates. Saadatfara *et al.* (2015) discussed conceptual modeling of nanofluid ORC for solar thermal polygeneration. Effects of radiation and chemical reaction on MHD unsteady heat and mass transfer of Casson fluid flow past a vertical plate has been discussed by Biswas *et al.* (2017).

Dufour and Soret effects on steady MHD free Convective flow past a vertical porous plate embedded in a porous medium with chemical reaction, radiation, heat generation and viscous dissipation has been introduced by Lavanya *et al.* (2014) and steady MHD natural convection flow with variable electrical conductivity and heat generation along an isothermal vertical plate has been observed Shrama *et al.* (2010). Also, Dogonchi *et al.* (2015) have introduced the investigation of heat transfer for cooling turbine disks with a non-newtonian fluid flow using DRA. Momentum and heat transfer behavior of Jeffrey, Maxwell and Oldroyd-B nanofluids past a stretching surface with non-uniform heat source/sink was submitted by Sandeep and Sulochana (2016). MHD boundary layer flow, heat and mass transfer analysis over a rotating disk through porous medium saturated by cu-water and ag-water nanofluid with chemical reaction has been premeditated by Reddy *et al.* (2017). Also, Cattaneo-Christov model for radiative heat transfer of magneto-hydrodynamic Casson-ferrofluid: A numerical study was found by Ali, and Sandeep (2017). Effect of variable viscosity, Dufour, Soret and thermal conductivity on free convection heat and mass transfer of non-Darcian flow past porous flat surface has been carried out by Animasaun, and Oyem (2014). Dufour and Soret effects on steady MHD free Convective flow past a vertical porous plate embedded in a porous medium with chemical reaction, radiation, heat generation and viscous dissipation was analyzed by Lavanya, and Ratnam (2014).

Magneto-hydrodynamic (MHD) is the branch of continuum mechanics which concerns with the flow of electrically conducting in electrical and magnetic fields. The flow of an electrically conducting fluid in the presence of a magnetic field is important in various area of technology. There are many applications of MHD free convection flows in fiber and granular insulation, geothermal systems etc. Unsteady MHD Casson fluid flow through a parallel plate with Hall current has been induced by Afikuzzaman *et al.* (2015). Also, MHD Casson fluid flow through a parallel plate has been elaborated by Afikuzzaman *et al.* (2016). MHD couette flow of a Casson fluid between parallel porous plates has been commenced by Wahiduzzaman *et al.* (2014). Effects of Hall current and chemical reaction on MHD unsteady heat and mass transfer of Casson nanofluid flow through a vertical plate was performed by Biswas *et al.* (2018). Unsteady magnetohydrodynamic free convection flow of nanofluid through an exponentially accelerated inclined plate embedded in a porous medium with variable thermal conductivity in the presence of radiation was recently published by Ahmmed *et al.* (2018). Effect of thermo-diffusion, Soret and heat generation effects, Radiation and chemical reaction effects on MHD etc. was presented by Kataria and Patel (2016, 2018). Also, Radiation effects on heat transfer of three dimensional nanofluid flow considering thermal interfacial resistance and micro mixing in suspensions has been introduced by Sheikholeslami *et al.* (2017). Furthermore, by Sheikholeslami *et al.* (2018) have described the effects of thermal

diffusion and heat-generation on MHD nanofluid flow past an oscillating vertical plate.

The aim has been carried out of this paper is to study the effects of chemical reaction on MHD unsteady heat and mass transfer flow through a vertical porous plate. In this paper we have scrutinized the effects of different parameters such as of magnetic parameter, permeability of porous medium, Eckert number, Pradlt number, Soret number, Schmidt number, heat source parameter, chemical reaction parameter, Grashof number, modified Grashof number and Dufour number on the fluid flow, temperature and concentration profiles. The model equations are solved numerically by explicit finite difference method (EFDM) and the obtained results are discussed with the help of graphs after stability test.

## 2. MATHEMATICAL ANALYSIS

The unsteady two dimensional free convection flow of an electrically conducting viscous incompressible fluid through a semi-infinite vertical porous permeable plate ( $y=0$ ) in the appearance of thermal diffusion, viscous dissipation, heat adsorption and chemical reaction is considered. Also, it is supposed that the  $x$ -axis is taken along the plate in the vertically upward direction and the  $y$ -axis is chosen normal to the plate. A uniform magnetic field of strength  $B_0$  is applied across to the flow direction which is arrested to be electrically non-conducting. This assuredness is justified when the Reynolds number is taken very small so that induced magnetic field strength ignored and is of the form  $B=(0, B_0, 0)$  where magnetic lines of force are fixed similar to the fluid. At initially, it is considered that the temperature of the wall is  $T_w$  and concentration at the plate is  $C_w$  which are constant but at time  $t>0$ , the plate is accelerated with a uniform velocity  $u=U_0$  in its own plane and the temperature and concentration level of the plate are raised as  $T_w(=T_\infty)$  and  $C_w(=C_\infty)$  respectively with time  $t$ . Mainly, the Dufour effects, Soret effects and chemical reaction on fluid flow has been evaluated in this new research work. The physical configuration and coordinate system of this model is shown in the following Fig 1.

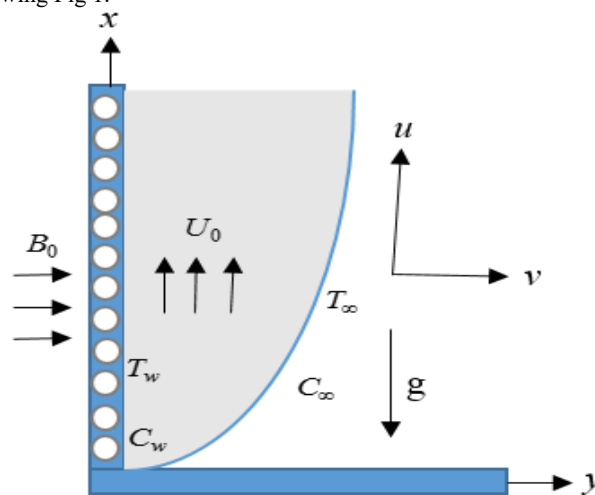


Fig. 1 Physical model and coordinate system

Under the assumptions made above, the governing dimensional continuity, momentum, energy and concentration equations respectively of the unsteady incompressible fluid flow with boundary conditions are follows

$$\frac{\partial u}{\partial x} + \frac{\partial v}{\partial y} = 0 \quad (1)$$

$$\frac{\partial u}{\partial t} + u \frac{\partial u}{\partial x} + v \frac{\partial u}{\partial y} = \nu \frac{\partial^2 u}{\partial y^2} + g\beta_T(T - T_\infty) + g\beta_C(C - C_\infty) - \frac{\nu}{k^*}u - \frac{\sigma B_0^2 u}{\rho} \quad (2)$$

$$\frac{\partial T}{\partial t} + u \frac{\partial T}{\partial x} + v \frac{\partial T}{\partial y} = \frac{k}{\rho C_p} \frac{\partial^2 T}{\partial y^2} + \frac{Q}{\rho C_p} (T - T_\infty) + \frac{D_m k_T}{C_s C_p} \frac{\partial^2 C}{\partial y^2} + \frac{\mu}{\rho C_p} \left( \frac{\partial u}{\partial y} \right)^2 \quad (3)$$

$$\frac{\partial C}{\partial t} + u \frac{\partial C}{\partial x} + v \frac{\partial C}{\partial y} = D_m \frac{\partial^2 C}{\partial y^2} - K_1 (C - C_\infty) + \frac{D_m K_T}{T_m} \frac{\partial^2 T}{\partial y^2} \quad (4)$$

The associate initial and boundary conditions according (5) to the model are

$$\left. \begin{aligned} u = U_0, v = 0, T = T_w, C = C_w \quad \text{at } y = 0 \\ u = 0, v = 0, T \rightarrow T_\infty, C \rightarrow C_\infty \quad \text{as } y \rightarrow \infty \end{aligned} \right\} \quad (5)$$

Here,  $u$  and  $v$  are the velocity components in the  $x$  and  $y$  axes respectively,  $\rho$  is the fluid density,  $T$  is the temperature of fluid,  $\nu$  is the kinematic viscosity,  $k$  is the thermal conductivity,  $D_m$  is the molecular diffusivity of the species concentration,  $\mu$  is dynamic viscosities,  $g$  is acceleration due to gravity,  $\sigma$  is Stefan-Boltzmann constant,  $K^*$  is Darcy permeability,  $T_m$  is the mean fluid temperature,  $g$  is the gravitational acceleration,  $k_1$  is the reaction rate constant,  $\beta_T$  is the thermal expansion coefficient,  $\beta_c$  is the concentration expansion coefficient,  $C_p$  is the specific heat at constant pressure,  $C_s$  is concentration susceptibility and  $k_T$  is the thermal diffusion ratio. The dimensionless governing equations have been obtained by applying the following dimensionless variables as

$$\begin{aligned} U = \frac{u}{U_0}; \quad V = \frac{v}{U_0}; \quad Y = \frac{yU_0}{\nu}; \quad X = \frac{xU_0}{\nu} \\ T = T_\infty + \bar{T}(T_w - T_\infty); \quad C = C_\infty + \bar{C}(C_w - C_\infty) \\ S = \frac{Q\nu}{\rho C_p U_0^2}; \quad M = \frac{\sigma B_0^2 \nu}{\rho U_0^2}; \quad S_c = \frac{\nu}{D_m} \\ S_r = \frac{D_m K_T}{T_m \nu} \frac{(T_w - T_\infty)}{(C_w - C_\infty)}; \quad K_p = \frac{\nu^2}{k^* U_0^2} \\ \gamma = \frac{K_1 \nu}{U_0^2}; \quad P_r = \frac{\nu \rho C_p}{k}; \quad E_c = \frac{U_0^2}{C_p (T_w - T_\infty)} \\ G_r = \frac{\nu g \beta_T (T_w - T_\infty)}{U_0^3}; \quad G_m = \frac{\nu g \beta_c (C_w - C_\infty)}{U_0^3} \\ D_u = \frac{D_m K_T}{C_s C_p \nu} \frac{(C_w - C_\infty)}{(T_w - T_\infty)} \end{aligned}$$

Therefore, the dimensionless governing equations are

$$\frac{\partial U}{\partial X} + \frac{\partial V}{\partial Y} = 0 \quad (6)$$

$$\begin{aligned} \frac{\partial U}{\partial \tau} + U \frac{\partial U}{\partial X} + V \frac{\partial U}{\partial Y} = \frac{\partial^2 U}{\partial Y^2} + G_r \bar{T} + G_m \bar{C} \\ - K_p U - M U \end{aligned} \quad (7)$$

$$\begin{aligned} \frac{\partial \bar{T}}{\partial \tau} + U \frac{\partial \bar{T}}{\partial X} + V \frac{\partial \bar{T}}{\partial Y} = \frac{1}{P_r} \frac{\partial^2 \bar{T}}{\partial Y^2} + S \bar{T} + D_u \frac{\partial^2 \bar{C}}{\partial Y^2} \\ + E_c \left( \frac{\partial U}{\partial Y} \right)^2 \end{aligned} \quad (8)$$

$$\frac{\partial \bar{C}}{\partial \tau} + U \frac{\partial \bar{C}}{\partial X} + V \frac{\partial \bar{C}}{\partial Y} = \frac{1}{S_c} \frac{\partial^2 \bar{C}}{\partial Y^2} - \gamma \bar{C} + S_r \frac{\partial^2 \bar{T}}{\partial Y^2} \quad (9)$$

Also, the associate boundary conditions according to the present model are

$$\left. \begin{aligned} U = 1, V = 0, \bar{T} = 1, \bar{C} = 1 \quad \text{at } Y = 0 \\ U = 0, \bar{T} \rightarrow 0, \bar{C} \rightarrow 0 \quad \text{as } Y \rightarrow \infty \end{aligned} \right\} \quad (10)$$

where,  $U, \bar{T}$  and  $\bar{C}$  represents the dimensionless velocity, temperature and concentration respectively,  $E_c$  is Eckert number,  $G_r$  is Grashof number,  $G_m$  is modified Grashof number,  $S_c$  is Schmidt number,  $S$  is heat source parameter,  $P_r$  is Prandlt number,  $K_p$  is permeability of porous medium,  $M$  is magnetic parameter,  $D_u$  is Dufour Number,  $\gamma$  is chemical reaction parameter and  $S_r$  is Soret number. The following non-dimensional quantities represents the skin friction coefficient ( $C_f$ ), Nusselt number ( $N_u$ ) and Sherwood number ( $S_h$ ) respectively as

$$C_f = -\frac{1}{2\sqrt{2}} (G_r)^{-\frac{3}{4}} \left( \frac{\partial U}{\partial Y} \right)_{Y=0}$$

$$N_u = \frac{1}{\sqrt{2}} (G_r)^{-\frac{3}{4}} \left( \frac{\partial \bar{T}}{\partial Y} \right)_{Y=0}$$

$$S_h = \frac{1}{\sqrt{2}} (G_r)^{-\frac{3}{4}} \left( \frac{\partial \bar{C}}{\partial Y} \right)_{Y=0}$$

Stream function  $\psi(X, Y)$  satisfies the continuity equation (10) and is associated with the velocity components in the usual way as:

$$U = \frac{\partial \psi}{\partial Y}, \quad V = -\frac{\partial \psi}{\partial X}$$

### 3. CALCULATION TECHNIQUE

To obtain the difference equations, the region of the flow is divided into a grid or mesh of lines parallel to  $X$  and  $Y$  axis where  $X$ - axis is taken along the plate and  $Y$ -axis is normal to the plate. It is considered that the plate of height  $X_{max}(=125)$  i.e.  $X$  varies from 0 to 125 and regard  $Y_{max}(=150)$  i.e.  $Y$  varies from 0 to 150. There are  $m=150$  and  $n=300$  grid spacing in the  $X$  and  $Y$  directions respectively as shown in Fig. 1(a).

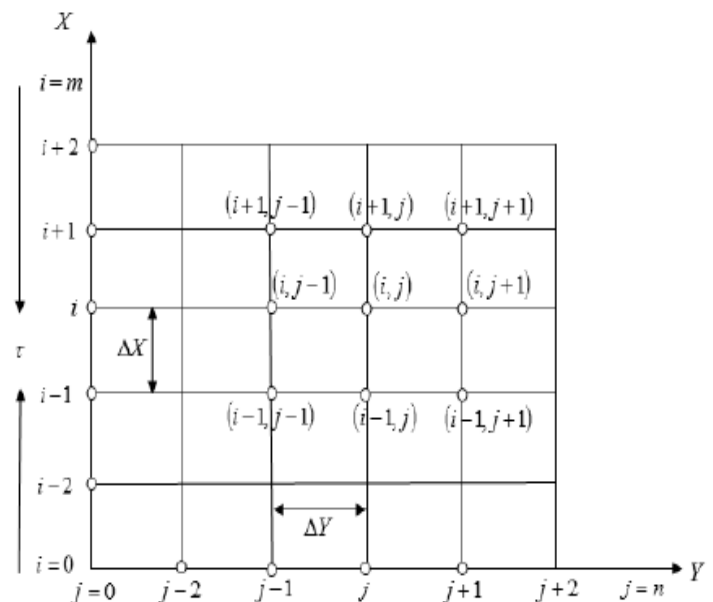


Fig. 2 The finite difference space grid

It is assumed that  $\Delta X, \Delta Y$  are constant mesh sizes along  $X$  and  $Y$  directions respectively and taken as follows  $\Delta X = 0.83(0 \leq x \leq 125)$ ;  $\Delta Y = 0.50(0 \leq y \leq 150)$ . With the smaller time-step,  $\Delta \tau = 0.0005$  and  $U', \bar{T}'$  and  $\bar{C}'$  denote the values of  $U, \bar{T}$  and  $\bar{C}$  at the end of a time-step respectively.

Therefore, the nonlinear coupled partial differential equation (6) to (9) with respect to the boundary conditions (10) are solved numerically by using explicit finite difference method as below

$$\frac{U_{i,j} - U_{i-1,j}}{\Delta X} + \frac{V_{i,j} - V_{i,j-1}}{\Delta Y} = 0 \quad (11)$$

$$\begin{aligned} \frac{U'_{i,j} - U_{i,j}}{\Delta \tau} + U_{i,j} \left( \frac{U_{i,j} - U_{i-1,j}}{\Delta X} \right) + V_{i,j} \left( \frac{U_{i,j+1} - U_{i,j}}{\Delta Y} \right) \\ = \left( \frac{U_{i,j+1} - 2U_{i,j} + U_{i,j-1}}{(\Delta Y)^2} \right) + G_r \bar{T}_{i,j} \\ + G_m \bar{C}_{i,j} - k_p U_{i,j} - M U_{i,j} \end{aligned} \quad (12)$$

$$\begin{aligned} \frac{\bar{T}'_{i,j} - \bar{T}_{i,j}}{\Delta \tau} + U_{i,j} \left( \frac{\bar{T}_{i,j} - \bar{T}_{i-1,j}}{\Delta X} \right) + V_{i,j} \left( \frac{\bar{T}_{i,j+1} - \bar{T}_{i,j}}{\Delta Y} \right) \\ = \frac{1}{P_r} \frac{\bar{T}_{i,j+1} - 2\bar{T}_{i,j} + \bar{T}_{i,j-1}}{(\Delta Y)^2} + S \bar{T}_{i,j} \\ + D_u \frac{\bar{C}_{i,j+1} - 2\bar{C}_{i,j} + \bar{C}_{i,j-1}}{(\Delta Y)^2} + E_c \left( \frac{U_{i,j+1} - U_{i,j}}{\Delta Y} \right)^2 \end{aligned} \quad (13)$$

$$\begin{aligned} \frac{\bar{C}'_{i,j} - \bar{C}_{i,j}}{\Delta \tau} + U_{i,j} \left( \frac{\bar{C}_{i,j} - \bar{C}_{i-1,j}}{\Delta X} \right) + V_{i,j} \left( \frac{\bar{C}_{i,j+1} - \bar{C}_{i,j}}{\Delta Y} \right) \\ = \frac{1}{S_c} \frac{\bar{C}_{i,j+1} - 2\bar{C}_{i,j} + \bar{C}_{i,j-1}}{(\Delta Y)^2} - \gamma \bar{C}_{i,j} \\ + S_r \frac{\bar{T}_{i,j+1} - 2\bar{T}_{i,j} + \bar{T}_{i,j-1}}{(\Delta Y)^2} \end{aligned} \quad (14)$$

In this case, the associate boundary conditions according to the present problem are:

$$\left. \begin{aligned} U_{i,0}^n = 1, V_{i,0}^n = 0, \bar{T}_{i,0}^n = 1, \bar{C}_{i,0}^n = 1 \\ U_{i,L}^n = 0, \bar{T}_{i,L}^n \rightarrow 0, \bar{C}_{i,L}^n \rightarrow 0 \text{ where } L \rightarrow \infty \end{aligned} \right\} \quad (15)$$

#### 4. STABILITY AND CONVERGENCE ANALYSIS

The stability conditions for the present problem are,

$$\frac{2\Delta \tau}{(\Delta Y)^2} + \frac{M\Delta \tau}{2} + U \frac{\Delta \tau}{\Delta X} + | -V | \frac{\Delta \tau^2}{\Delta Y} + \frac{K_p \Delta \tau}{2} \leq 1 \quad (16)$$

$$\frac{1}{P_r} \frac{2\Delta \tau}{(\Delta Y)^2} + U \frac{\Delta \tau}{\Delta X} + | -V | \frac{\Delta \tau}{\Delta Y} - \frac{S \Delta \tau}{2} \leq 1 \quad (17)$$

$$\frac{1}{S_c} \frac{2\Delta \tau}{(\Delta Y)^2} + \frac{\gamma \Delta \tau}{2} + U \frac{\Delta \tau}{\Delta X} + | -V | \frac{\Delta \tau}{\Delta Y} \leq 1 \quad (18)$$

Using initial condition,  $U=V=0$  at  $\tau=0$  in the equations (16) to (18), then the convergence criteria of the present problem are obtained as  $P_r \geq$

$0.034$  and  $S_c \geq 0.035$  respectively for stable solutions. Therefore, the convergence criteria of the present problem are  $P_r \geq 0.034$  and  $S_c \geq 0.035$ .

#### 5. RESULTS AND DISCUSSION

An explicit finite difference technique has been used to obtain the numerical results of the present model and the physical situation of the present model has been carried out for the difference values of various parameters on velocity, temperature, concentration, skin friction coefficient, Nusselt number, Sherwood number, streamlines and isotherms through a vertical porous permeable plate within the boundary conditions. The numerical results which are obtained for different values of permeability of porous medium ( $K_p$ ), Eckert number ( $E_c$ ), Soret number ( $S_r$ ), magnetic parameter ( $M$ ), Schmidt number ( $S_c$ ), Prandtl number ( $P_r$ ), heat source parameter ( $S$ ), chemical reaction parameter ( $\gamma$ ), Grashof number ( $G_r$ ), modified Grashof number ( $G_m$ ) and Dufour number ( $D_u$ ) and all are shown in the Figs. 3-18. In order to obtain the numerical results, the following values of default parameter are chosen as:  $M=0.50, P_r=0.63, S_c=0.22, E_c=0.01, D_u=0.50, S=0.1, S_r=1, G_m=5, G_r=10, K_p=1.0$ , and  $\gamma=0.50$  with time  $\tau=10$ . These all values are treated as common throughout the study in respective Figs and Tables.

The effects of different values of magnetic parameter ( $M$ ), chemical reaction ( $\gamma$ ) and Grashof number ( $G_r$ ) on velocity are premeditated in the Figs. 3-5 respectively. From Fig. 3, we have seen that velocity decreases with the increase of magnetic parameter ( $M$ ). This is why, by increasing magnetic parameter which produce a resistive Lorentz force in the fluid flow and this force decreased the velocity profiles. Also, velocity decreases due to the increases of chemical reaction ( $\gamma$ ) which occurs in Fig. 4. Physically, chemical reaction parameter leads to downfall of velocity and concentration because the positive values of chemical reaction parameter ( $\gamma > 0$ ) predicts the effects of destructive chemical reaction on the concentration field. Physically for generative case, chemical reaction  $\gamma$  takes place without creating much disturbance whereas in the case of destructive chemical reaction is much larger. But, in Fig. 5 velocity increases due the increase of Grashof number ( $G_r$ ), because the thermal Grashof number which signifies the relative effect of the thermal buoyancy force in the boundary layer. Due to this enhancement of thermal buoyancy force which acting on the fluid particles for gravitational force that increases the primary and secondary velocity.

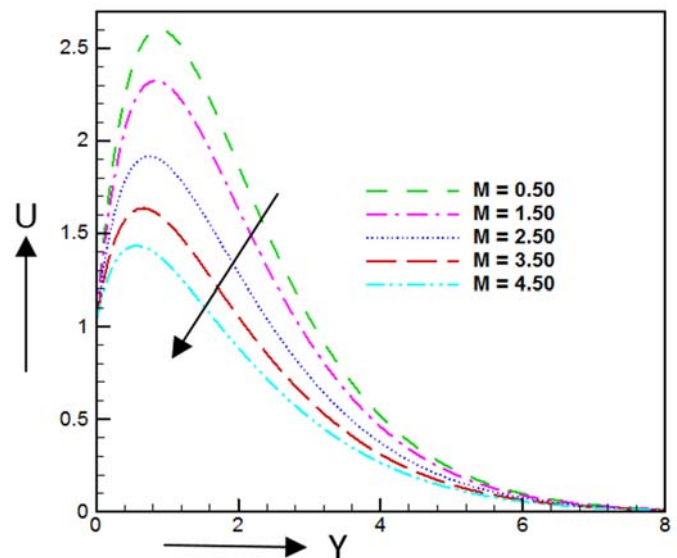


**Fig. 3** Velocity profiles for different values of  $M$  against  $Y$  when  $K_p=1.0, P_r=0.63, S_c=0.22, E_c=0.01, S_r=1.0, S=0.10, \gamma=0.50, G_r=10, G_m=5$  and  $D_u=0.5$ .

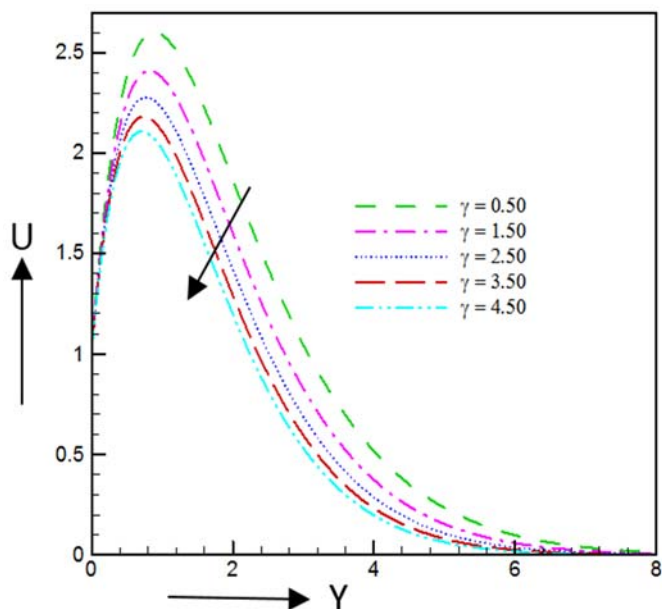


**Fig. 4** Velocity profiles for different values of  $\gamma$  against  $Y$  when  $M=1.0$ ,  $K_p=1.0$ ,  $P_r=0.63$ ,  $S_c=0.22$ ,  $E_c=0.01$ ,  $S_r=1.0$ ,  $S=0.10$ ,  $G_r=10$ ,  $G_m=5$  and  $D_u=0.5$ .

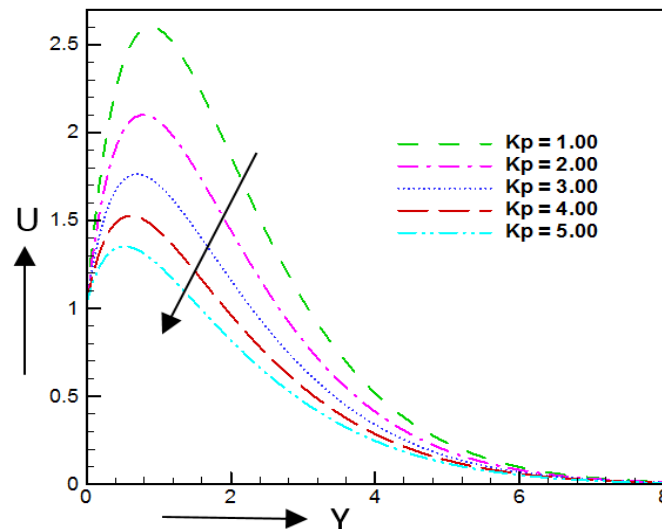


**Fig. 6** Velocity profiles for different values of  $K_p$  against  $Y$  when  $M=1.0$ ,  $P_r=0.63$ ,  $S_c=0.22$ ,  $E_c=0.01$ ,  $S_r=1.0$ ,  $S=0.10$ ,  $\gamma=0.50$ ,  $G_r=10$ ,  $G_m=5$  and  $D_u=0.5$ .

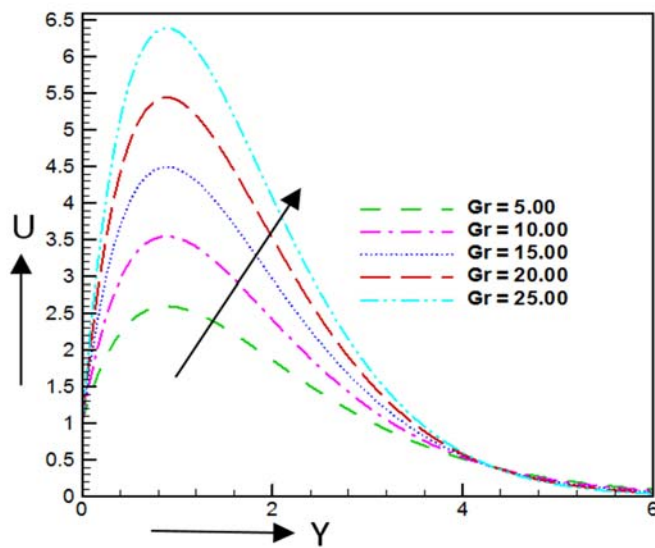


**Fig. 5** Velocity profiles for different values of  $G_r$  against  $Y$  when  $M=1.0$ ,  $K_p=1.0$ ,  $P_r=0.63$ ,  $S_c=0.22$ ,  $E_c=0.01$ ,  $S_r=1.0$ ,  $S=0.10$ ,  $\gamma=0.50$ ,  $G_m=5$  and  $D_u=0.5$ .

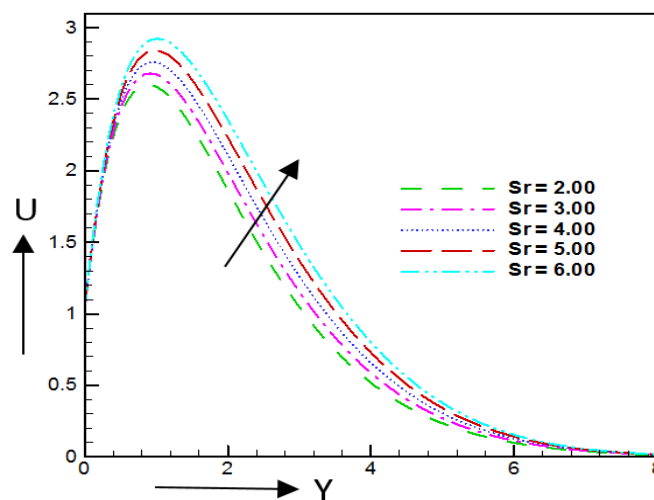


**Fig. 7** Velocity profiles for different values of  $S_r$  against  $Y$  when  $M=1.0$ ,  $K_p=1.0$ ,  $P_r=0.63$ ,  $S_c=0.22$ ,  $E_c=0.01$ ,  $S=0.10$ ,  $\gamma=0.50$ ,  $G_r=10$ ,  $G_m=5$  and  $D_u=0.5$ .

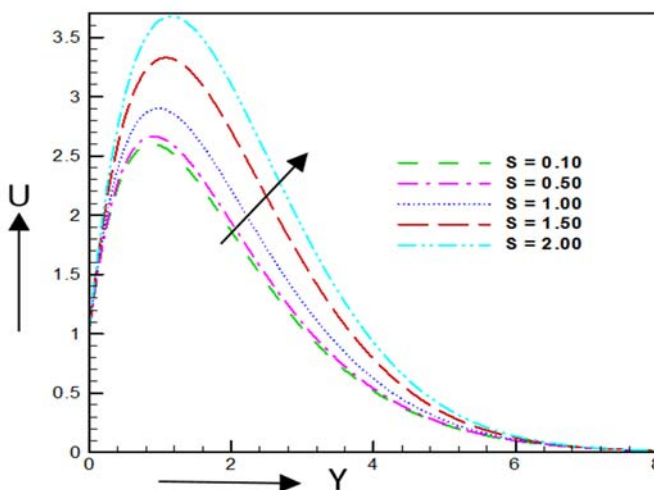


**Fig. 8** Velocity profiles for different values of  $S$  against  $Y$  when  $M=1.0$ ,  $K_p=1.0$ ,  $P_r=0.63$ ,  $S_c=0.22$ ,  $E_c=0.01$ ,  $S_r=1.0$ ,  $\gamma=0.50$ ,  $G_r=10$ ,  $G_m=5$  and  $D_u=0.5$ .

The effects of permeability of porous medium ( $K_p$ ), Soret number ( $S_r$ ) and heat source parameter ( $S$ ) are obtained in the following Fig. 6-8 respectively. It is concluded that from Fig. 6 velocity decreases 59.49%, 50.4%, 45.2% and 32.50% for  $K_p=1.0$  to  $K_p=2.0$ ,  $K_p=2.0$  to  $K_p=3.0$ ,  $K_p=3.0$  to  $K_p=4.0$  and  $K_p=4.0$  to  $K_p=5.0$  at  $Y=0.4556$ . Generally, the presence of porous medium which increase a resistive force in the flow of fluid and this resistive force decreased the velocity distributions. On the other hand velocity increases due to increases of Soret number ( $S_r$ ) and heat source parameter ( $S$ ) respectively which occurs in Figs. 7 and 8. Soret number and heat generation parameter enhances the velocity profiles thereby increasing the momentum boundary layer thickness. Furthermore, Heat generation parameter enhances the temperature profiles thereby increasing the thermal boundary layer thickness. For this reasons, velocity increases due to the increase of Soret number and heat generation parameter.

The heat source parameter ( $S$ ), Prandtl number ( $Pr$ ), Eckert number ( $Ec$ ) and Dufour number ( $Du$ ) on temperature profiles are shown in the Figs. 9-12. It is worth mentioned that from Fig. 9, temperature profiles increases with the increase of heat source parameter ( $S$ ). Physically, heat generation parameter enhances the temperature profiles thereby increasing the thermal boundary layer thickness such that enhance the temperature profiles. But on the other hand it is seen that temperature profiles are decreased by 34.49%, 25%, 22.4% and 15.50% for  $Pr=0.63$  to  $Pr=1.00$ ,  $Pr=1.00$  to  $Pr=1.38$ ,  $Pr=1.38$  to  $Pr=7.00$  and  $Pr=7.00$  to  $Pr=11.62$  respectively which are shown in Fig. 10. Naturally, this is due to the fluid with high Prandtl number have greater viscosity, which decreases thermal boundary layer thickness i.e. for decreasing thermal boundary layer, heat transfer is reduced. By increasing the Eckert number the heat energy is stored in the fluid due to the frictional or drag forces. So, the fluid temperature increases by the increasing of Eckert number which is shown in the Fig. 11. Also, the effect of the Dufour number on the temperature profiles is permitted in the Fig. 12. It is observed that by increasing  $Du$  parameter leads to a decrease the temperature profiles.

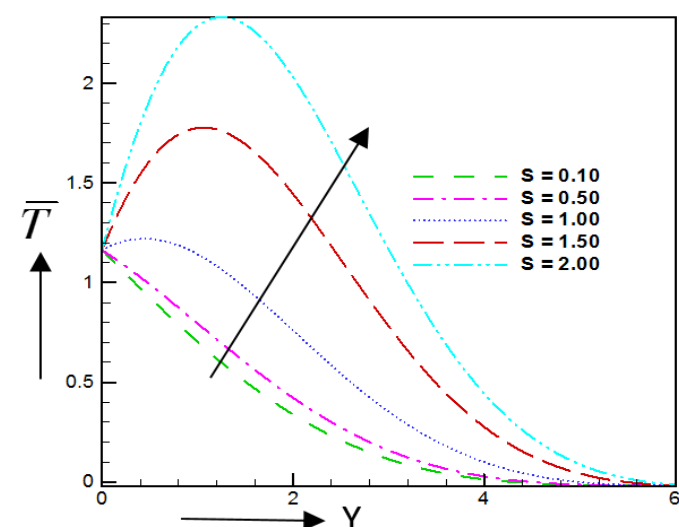


**Fig. 9** Temperature profiles for different values of  $S$  against  $Y$  when  $M=1.0$ ,  $K_p=1.0$ ,  $Pr=0.63$ ,  $Sc=0.22$ ,  $Ec=0.01$ ,  $S_r=1.0$ ,  $\gamma=0.50$ ,  $G_r=10$ ,  $G_m=5$  and  $Du=0.5$ .

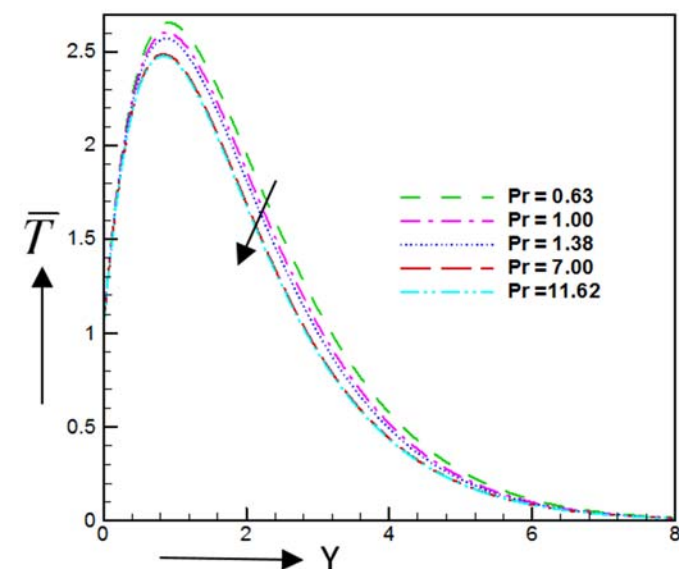


**Fig. 10** Temperature profiles for different values of  $Pr$  against  $Y$  when  $M=1.0$ ,  $K_p=1.0$ ,  $Sc=0.22$ ,  $Ec=0.01$ ,  $S_r=1.0$ ,  $S=0.10$ ,  $\gamma=0.50$ ,  $G_r=10$ ,  $G_m=5$  and  $Du=0.5$ .

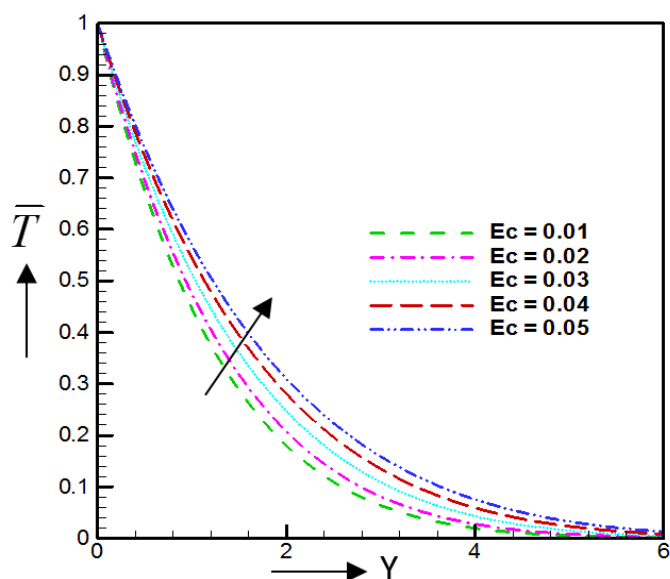


**Fig. 11** Temperature profiles for different values of  $Ec$  against  $Y$  when  $M=1.0$ ,  $K_p=1.0$ ,  $Pr=0.63$ ,  $Sc=0.22$ ,  $S_r=1.0$ ,  $S=0.10$ ,  $\gamma=0.50$ ,  $G_r=10$ ,  $G_m=5$  and  $Du=0.5$ .

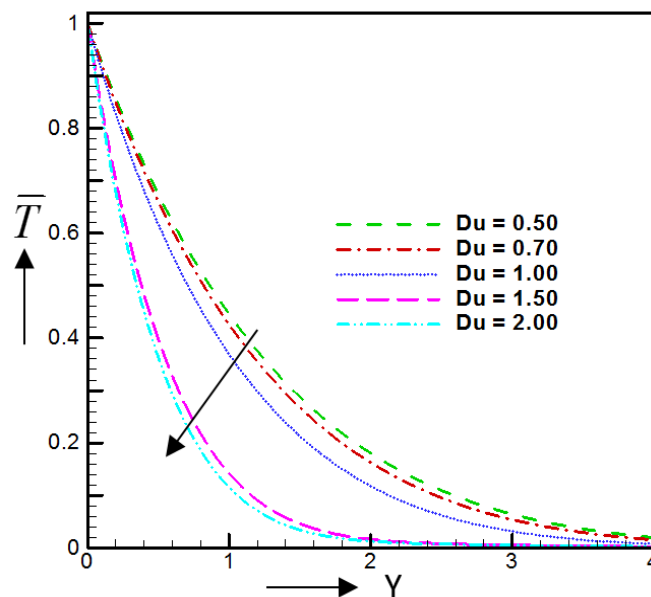


**Fig. 12** Temperature profiles for different values of  $Du$  against  $Y$  when  $M=1.0$ ,  $K_p=1.0$ ,  $Pr=0.63$ ,  $Sc=0.22$ ,  $Ec=0.01$ ,  $S_r=1.0$ ,  $S=0.10$ ,  $\gamma=0.50$ ,  $G_r=10$  and  $G_m=5$ .

Also, the influence of Schmidt number ( $Sc$ ) and chemical reaction ( $\gamma$ ) on concentration profiles are extracted in Figs. 13 and 14. From Fig. 13 this is fact that, the indulgent motion of nanoparticles get decreased with an increase in Schmidt number  $Sc$ . Physically, It is known that, Schmidt number ( $Sc$ ) is a dimensionless number defined as the ratio of viscous diffusivity to mass diffusivity, this is why by increasing Schmidt number which increase the mass diffusivity and this mass diffusivity decreased the concentration profiles. Further chemical reaction ( $\gamma$ ) decreased the concentration profiles which are showed in Fig. 14. It can be observed that chemical reaction parameter reduces the concentration boundary layers. Due to an increase in the interfacial mass transfer which decreased the concentration profiles. Also, It can be observed from the figures that a rise in the value of chemical reaction parameter ( $\gamma$ ) reduces the concentration boundary layers. Due to an increase in the interfacial mass transfer we observed a fall in concentration profiles.

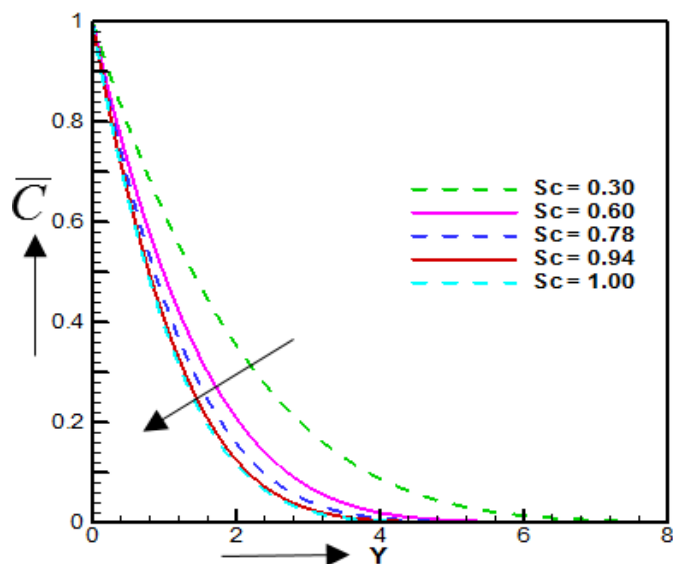


**Fig. 13** Concentration profiles for different values of  $Sc$  against  $Y$  when  $M=1.0$ ,  $K_p=1.0$ ,  $P_r=0.63$ ,  $E_c=0.01$ ,  $S_r=1.0$ ,  $S=0.10$ ,  $\gamma=0.50$ ,  $G_r=10$ ,  $G_m=5$  and  $D_u=0.5$ .

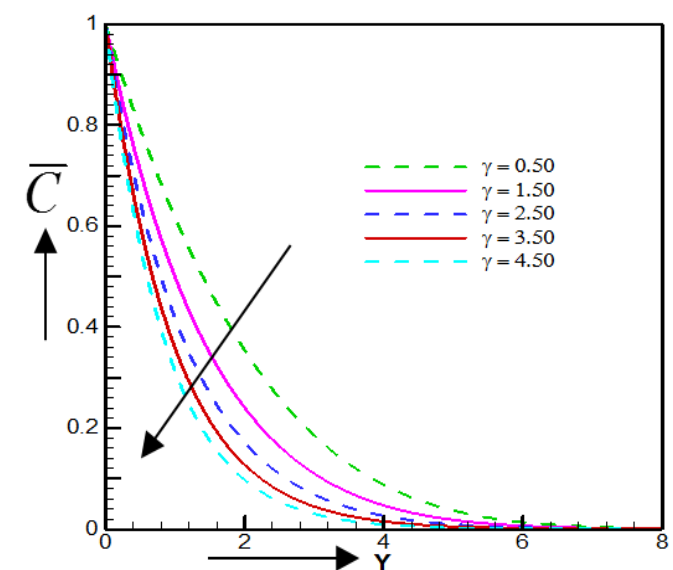


**Fig. 14** Concentration profiles for different values of  $\gamma$  against  $Y$  when  $M=1.0$ ,  $K_p=1.0$ ,  $P_r=0.63$ ,  $Sc=0.22$ ,  $E_c=0.01$ ,  $S_r=1.0$ ,  $S=0.10$ ,  $G_r=10$ ,  $G_m=5$  and  $D_u=0.5$ .

The dimensionless equations are transformed by the as usual procedure of transformation and solved it numerically. Therefore, for this reason,  $X$  and  $Y$  axis are dimensionless which indicates the mesh point different from the numerical point of view. Also, with the stream and isotherms (line view) curves, the difference of boundary layer for different parameters can be defined. The impact of magnetic parameter ( $M$ ) on streamlines and isotherms are represented in Fig. 15 and Fig. 16. The momentum boundary layer thickness increases and thermal boundary layer thickness decreases due to increase of magnetic parameter  $M=0.50$  to  $M=1.00$ . Also, the effect of chemical reaction ( $\gamma$ ) on streamlines and isotherms are represented in Fig. 17 and Fig. 18. Here, we observed that momentum boundary layer thickness and thermal boundary layer thickness both are increasing due to the increase of chemical reaction from  $\gamma=0.50$  to  $\gamma=1.50$ .

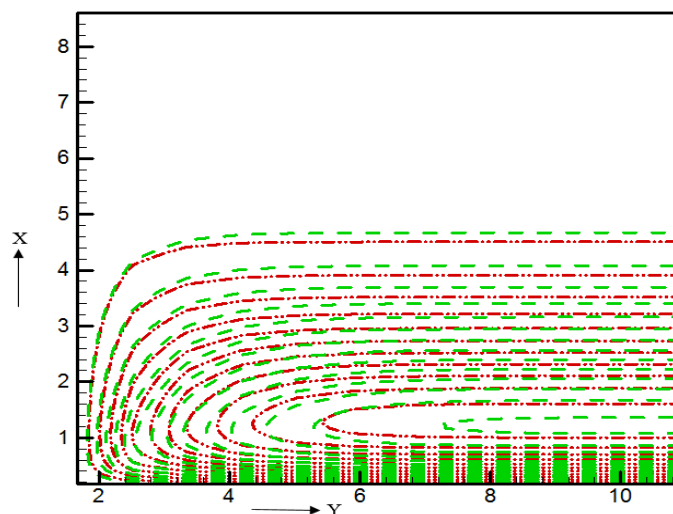


**Fig. 15** Isotherms for  $M=0.50$  (red dashed dot dot line) and  $M=1.00$  (green dashed line).

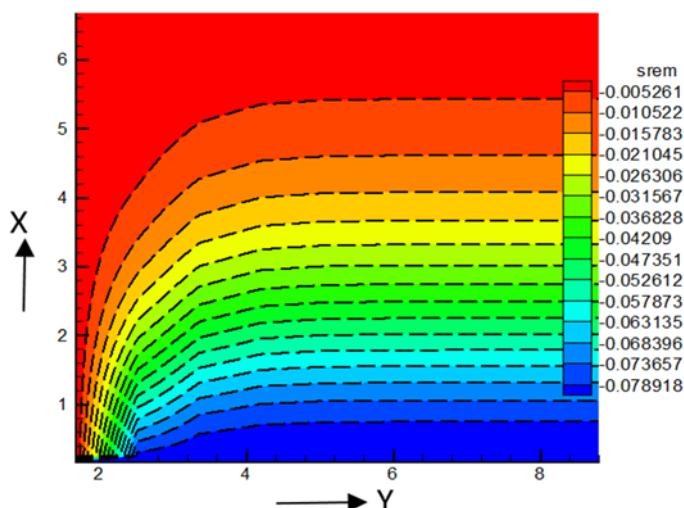


**Fig. 16** Streamlines for  $M=0.50$  and  $M=1.00$  (black dashed line with flood view).

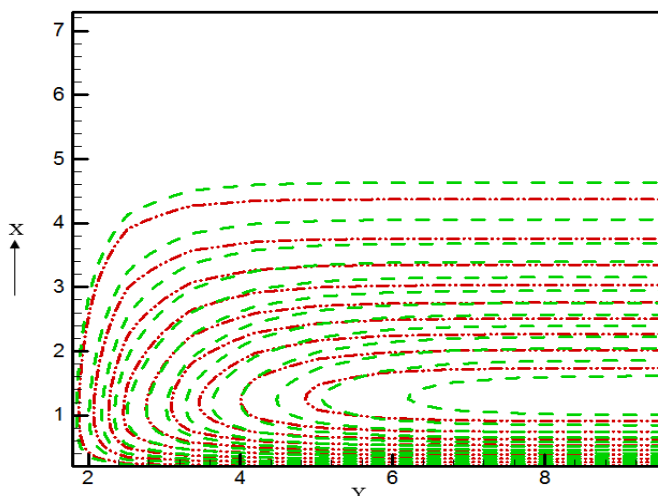


**Fig. 17** Isotherms for  $\gamma=0.50$  (red dashed dot dot line) and  $\gamma=1.50$  (green dashed line).

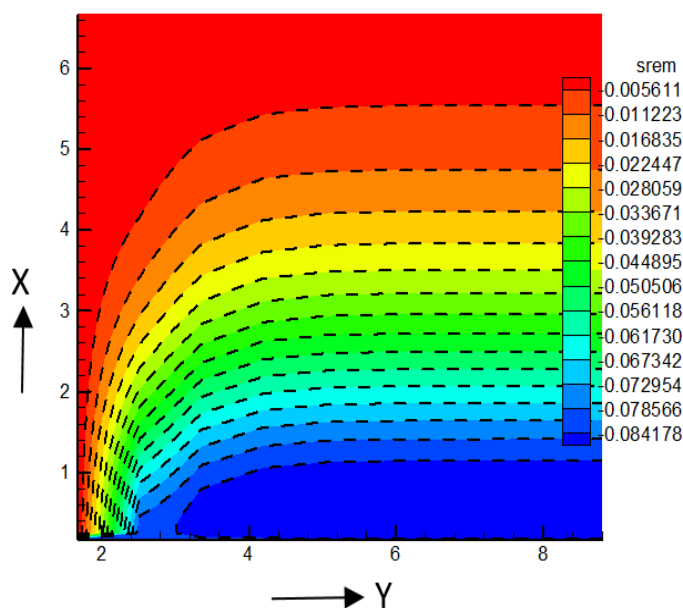


**Fig. 18** Streamlines for  $\gamma=0.50$  and  $\gamma=1.50$  (black dashed line with flood view).

**Table 1** and **Table 2** represents the variation of different parameters on skin friction coefficient, Nusselt number and Sherwood number. For various values of permeability of porous medium  $K_p$  on skin friction coefficient, Nusselt number and Sherwood number are delimited in Table 1. It is observed that skin friction coefficient decreased by 0.65% and 0.55% as permeability of porous medium  $K_p$  changes from 1.00 to 1.50 and 1.50 to 2.50 respectively at  $Y=0.5764$ . Physically, skin friction which is increased the rate of velocity of the fluid flow. Also, Nusselt number increases by 0.14% and 0.36% as permeability of porous medium  $K_p$  changes from 1.00 to 1.50 and 1.50 to 2.50 respectively at  $Y=0.5775$  but there is no effect on Sherwood number. In this case we observed that skin friction coefficient decreases to 4.39% and 3.28% but Nusselt number increases to 23.75% and 20.10% at  $Y=0.3545$  as Prandtl number changes from 0.63 to 0.71 and 0.71 to 1.00 respectively which occurs at time  $\tau=1$ . This is why which increase the conductive heat transfer and this is due to fact which decrease the Nusselt number. Also, it is clear that, skin friction coefficient increases but Nusselt number decreases as Soret number  $S_r$  changes from 2.00 to 3.00 and 3.00 to 4.00. On the other hand skin friction coefficient and Nusselt number decreases but Sherwood number increases from  $S_c=0.22$  to  $S_c=0.60$  and  $S_c=0.60$  to  $S_c=0.78$  respectively. Furthermore, we observed from Table 2 skin friction coefficient decreased by 1.10% and 1.05% as magnetic parameter changes from  $M=0.50$  to  $M=0.70$  and  $M=0.70$  to  $M=0.90$  respectively which occurs at time  $\tau=1$  but Nusselt number increases due to increasing of magnetic parameter. From Table 2, we conclude that skin friction coefficient increased by 6.30% and 4.20% as Dufour number changes from 0.5 to 1.00 and 1.00 to 1.50 respectively which occurs at time  $\tau=1$  but Nusselt number decreases. It is noted that increasing in chemical reaction parameter  $\gamma$  increases the skin friction coefficient and Sherwood number but Nusselt number decreased. Generally, convective mass transfer is increased with the increase of Sherwood number but when it is decreased then the opposite observations are happens. In the **Table 2** skin friction coefficient increased by 0.29% and 0.22% as Grashof number changes as 5 to 10 and 10 to 15 respectively which occurs at  $Y=0.533$  but Nusselt number and Sherwood number decreases for increasing Grashof number.

**Table 1.** Variation of different parameters ( $K_p, Pr, Sr$  and  $Sc$ ) on skin friction coefficient, Nusselt number and Sherwood number.

$K_p$	$Pr$	$S_r$	$Sc$	$C_f$	$Nu$	$Sh$
<b>1.00</b>	0.63	2.00	0.22	0.12123	0.36731	0.23310
<b>1.50</b>	0.63	2.00	0.22	0.11478	0.36738	0.23310
<b>2.50</b>	0.63	2.00	0.22	0.10930	0.36744	0.23310
0.50	<b>0.63</b>	2.00	0.22	0.12160	0.35241	0.22797
0.50	<b>0.71</b>	2.00	0.22	0.11809	0.37139	0.22797
0.50	<b>1.00</b>	2.00	0.22	0.10861	0.42965	0.22797
0.50	0.63	<b>2.00</b>	0.22	0.11974	0.35555	0.22219
0.50	0.63	<b>3.00</b>	0.22	0.12493	0.32913	0.22219
0.50	0.63	<b>4.00</b>	0.22	0.13225	0.29576	0.22219
0.50	0.63	2.00	<b>0.22</b>	0.11889	0.35705	0.22329
0.50	0.63	2.00	<b>0.60</b>	0.11698	0.35363	0.31579
0.50	0.63	2.00	<b>0.78</b>	0.11633	0.35183	0.36007

**Table 2.** Variation of different parameters ( $M, Du, \gamma$  and  $Gr$ ) on skin friction coefficient, Nusselt number and Sherwood number.

$M$	$Du$	$\gamma$	$Gr$	$C_f$	$Nu$	$Sh$
<b>0.50</b>	0.50	0.50	5.00	0.11726	0.36075	0.22686
<b>0.70</b>	0.50	0.50	5.00	0.11505	0.36078	0.22686
<b>0.90</b>	0.50	0.50	5.00	0.11296	0.36080	0.22686
0.50	<b>0.50</b>	0.50	5.00	0.11849	0.35776	0.22398
0.50	<b>1.00</b>	0.50	5.00	0.18148	0.35758	0.22398
0.50	<b>1.50</b>	0.50	5.00	0.22348	0.35750	0.22398
0.50	0.50	<b>0.50</b>	5.00	0.11950	0.35598	0.22225
0.50	0.50	<b>1.50</b>	5.00	0.14280	0.35261	0.30400
0.50	0.50	<b>2.50</b>	5.00	0.16257	0.34952	0.37442
0.50	0.50	0.50	<b>5.00</b>	0.11808	0.35848	0.22468
0.50	0.50	0.50	<b>10.00</b>	0.13273	0.21208	0.13359
0.50	0.50	0.50	<b>15.00</b>	0.14417	0.15519	0.09856

Comparison of the accuracy of the present results with the previous results by Kataria, H. R. and Patel (2018) are presented in the following Table 3 and Table 4. Here, it is permitted that, all values are same with the works of by Kataria, H. R. and Patel (2018).

**Table 3** represents the previous results by Kataria, H. R. and Patel (2018).

Previous results by Kataria, H. R. and Patel (2018).						
Increased parameters	$U$	$T$	$C$	Skin fri.	Nu. Num.	Sher. Num.
$G_r$						
$S$		In c				
$S_r$		In c				
$M$		Dec				
$\gamma$		Dec		Dec		In c
$E_c$						
$P_r$					In c	

**Table 4** represents the present results.

Our present results						
Increased parameters	$U$	$T$	$C$	Skin fri.	Nu. Num.	Sher. Num.
$G_r$	In c					
$S$	In c	In c				
$S_r$	In c					
$M$	Dec					
$\gamma$	Dec			Dec		In c
$E_c$	In c					
$P_r$		Dec			In c	

## 6. CONCLUSIONS

From the above investigation, the following conclusions have been drawn:

- It is observed that permeability of porous medium decreases the velocity profiles and skin-friction coefficient but Nusselt number is increased by  $K_p$ .
- An increase in chemical reaction parameter which increased the skin-friction coefficient.
- In view of that Prandtl number which decreases the skin friction coefficient but increased the Nusselt number.
- An increase in Schmidt number the temperature profiles are decreased.
- Velocity profiles are decreased with the increasing of magnetic parameter and Prandtl number.
- Chemical reaction decreased concentration profiles but Soret number increased the concentration profiles.

## NOMENCLATURE

$B_0$	Magnetic component ( $\text{Wbm}^{-2}$ )
$C$	Concentration of fluid (-)
$\bar{C}$	Dimensionless fluid concentration (-)
$C_f$	Skin friction (-)
$C_s$	Concentration susceptibility ( $\text{J/kg}\cdot\text{K}$ )
$C_p$	Specific heat at constant pressure ( $\text{J/m}^3\cdot\text{K}$ )
$D_m$	Molecular diffusivity of the concentration (-)
$D_u$	Dufour Number (-)
$E_c$	Eckert number (-)
$g$	Acceleration due to gravity ( $\text{ms}^{-2}$ )
$G_r$	Grashof number (-)
$G_m$	Modified Grashof number (-)
$k$	Thermal conductivity ( $\text{W/m}\cdot\text{K}$ )
$k_1$	Reaction rate constant (-)
$K_p$	Permeability of porous medium (-)
$K^*$	Darcy permeability (-)
$kr$	Thermal diffusion ratio (-)
$M$	Magnetic parameter (-)
$Nu$	Nusselt number (-)
$Pr$	Prandtl number (-)
$Q$	Heat absorption quantity (-)
$S$	Heat source parameter (-)
$Sc$	Schmidt number (-)
$Sh$	Sherwood number (-)
$S_r$	Soret number (-)
$T$	Temperature of fluid (K)
$T_w$	Temperature at the plate surface (K)
$T_\infty$	Temperature at far away from the plate (K)
$\bar{T}$	Dimensionless fluid temperature (K)
$T_m$	Mean fluid temperature (K)
$U$	Dimensionless primary velocity (m/s)
$U_0$	Uniform velocity (m/s)
$u, v$	Velocity components (m/s)
$x, y$	Cartesian coordinates (m)

### Greek Symbols

$\beta_r$	Thermal expansion coefficient (-)
$\mu$	Dynamic viscosities ( $\text{m}^2\text{s}^{-1}$ )

$\rho$	Fluid density ( $\text{kg/m}^3$ )
$\nu$	Kinematic viscosity ( $\text{m}^2\text{s}^{-1}$ )
$\beta_c$	Concentration expansion coefficient (-)
$\gamma$	Chemical reaction parameter (-)
$\sigma$	Stefan-Boltzmann constant ( $\text{W/m}^2\cdot\text{K}^4$ )

### Abbreviations

<i>PDEs</i>	Partial differential equations
<i>EFDM</i>	Explicit finite difference method
<i>SCT</i>	Stability convergence test
<i>CVF</i>	Compaq Visual FORTRAN
<i>MHD</i>	Magneto-hydrodynamic
<i>ODEs</i>	Ordinary differential equations

## REFERENCES

- Ahmed, N., Khan, U., Khan, S. I., Bano, S. and Mohyud-Din, S. T., 2017, "Effects on Magnetic Field in Squeezing Flow of a Casson Fluid between Parallel Plates," *Journal of King Saud University Science*, **29**, 119-125.  
<https://doi.org/10.1016/j.jksus.2015.03.006>
- Ali, M. E., and Sandeep, N., 2017, "Cattaneo-Christov Model for Radiative Heat Transfer of Magneto-hydrodynamic Casson-ferrofluid: A Numerical Study," *Results in Physics*, **7**, 21-30.  
<https://doi.org/10.1016/j.rinp.2016.11.055>
- Arani, A. G. and Zarei, M. S., 2015, "Nonlocal Vibration of y-Shaped CNT Conveying Nano-Magnetic Viscous Fluid under Magnetic Field," *Ain Shams Engineering Journal*, **6**, 565-575.  
<https://doi.org/10.1016/j.asej.2014.11.012>
- Animasaun, I. J., and Oyem, A. O., 2014, "Effect of Variable Viscosity, Dufour, Soret and Thermal Conductivity on Free Convection Heat and Mass Transfer of Non-Darcian Flow Past Porous Flat Surface," *American Journal of Computational Mathematics*, **33**, 271-292.  
<https://doi.org/10.1016/j.jnms.2014.10.008>
- Biswas, R., Mondal, M., Sarkar, D. R. and Ahmmmed, S. F., 2017, "Effects of Radiation and Chemical Reaction on MHD Unsteady Heat and Mass Transfer of Casson Fluid Flow Past a Vertical Plate," *Journal of Advances in Mathematics and Computer Science*, **23**(2), 1-16.  
<http://www.sciencedomain.org/review-history/19926>
- Bilal, S., Rehman, K. U., Malik, M. Y., 2017, "Hussain, A. and Awais, M., "Effect Logs of Double Diffusion on MHD Prandtl Nanofluid Adjacent to 4 Stretching Surface by Way of Numerical Approach," *Results in Physics*, **7**, 470-479.  
<https://doi.org/10.1016/j.rinp.2016.11.008>
- Das, S., Guchhait, S. K., Jana, R. N. and Makinde, O. D., 2016, "Hall Effects on an Unsteady Magneto-Convection and Radiative Heat Transfer past a Porous Plate," *Alexandria Engineering Journal*, **55**, 1321-1331.  
<https://doi.org/10.1016/j.aej.2016.04.027>
- Dogonchi, A.S., Ganji, D.D., 2015, "Investigation of Heat Transfer for Cooling Turbine Disks with a Non-Newtonian Fluid Flow Using DRA," *Case Studies in Thermal Engineering*, **6**, 40-51.  
<https://doi.org/10.1016/j.csite.2015.06.002>
- Dogonchi, A.S., Ganji, D.D., 2016, "Study of Nanofluid Flow and Heat Transfer between Non-parallel Stretching Walls Considering Brownian Motion," *Journal of the Taiwan Institute of Chemical Engineers*, **69**, 1-13.  
<https://doi.org/10.1016/j.jtice.2016.09.029>

Hossain, M. D., Samad, M. A. and Alam, M. M., 2015, "MHD Free Convection and Mass Transfer Flow Through a Vertical Oscillatory Porous Plate with Hall, Ion-slip Currents and Heat Source in a Rotating System," *Procedia Engineering*, **105**, 56-63.  
<https://doi.org/10.1016/j.proeng.2015.05.006>

Khalid, A., Khan, I., Khan, A. and Shafie, S., 2015, "Unsteady MHD Free Convection Flow of Casson Fluid past Over an Oscillating Vertical Plate Embedded in a Porous Medium," *Engineering Science and Technology*, **18**, 309-317.  
<https://doi.org/10.1016/j.jestch.2014.12.006>

Lavanya, B. and Ratnam, A. L., 2014, "Dufour and Soret effects on Steady MHD Free Convective Flow past a Vertical Porous Plate Embedded in a Porous Medium with Chemical Reaction, Radiation, Heat Generation and Viscous Dissipation," *Advances in Applied Science and Research*, **5**(1), 127-142.  
[www.imedpub.com/](http://www.imedpub.com/)

Mahanta, G. and Shaw, S., 2016, "3D Casson Fluid Flow past a Porous Linearly Stretching Sheet with Convective Boundary Condition," *Alexandria Engineering Journal*, **54**, 653-659.  
<https://doi.org/10.1016/j.aej.2015.04.014>

Oyelakin, I. S., Mondal, S. and Sibanda, P., 2016, "Unsteady Casson Nanofluid Flow Over a Stretching Sheet with Thermal Radiation, Convective and Slip Boundary Conditions," *Journal of the Nigerian Mathematical Society*, **34**, 11-31.  
<https://doi.org/10.1016/j.aej.2016.03.003>

Reddy, P. S., Sreedevi, P., and Chamkha, A. J., 2017, "MHD Boundary Layer Flow, Heat and Mass Transfer Analysis over a Rotating Disk Through Porous Medium Saturated by Cu-Water and Ag-Water Nanofluid with Chemical Reaction," *Powder Technology*, **307**, 46-55.  
<https://doi.org/10.1016/j.powtec.2016.11.017>

Ramesh, G.K., Gireesha, B.J., Hayat, T. and Alsaedi, A., 2016, "Stagnation Point Flow of Maxwell Fluid towards A Permeable Surface in the Presence of Nanoparticles," *Alexandria Engineering Journal*, **55**, 857-865.  
<https://doi.org/10.1016/j.aej.2016.02.007>

Seth, G. S., Sarkar, S. and Hussain, S. M., 2014, "Effects of Hall Current, Radiation and Rotation on Natural Convection Heat and Mass Transfer Flow past a Moving Vertical Plate," *Ain Shams Engineering Journal*, **5**, 489-503.  
<https://doi.org/10.1016/j.asej.2013.09.014>

Srikantha, G.V.P.N., Srinivasa, D.G. and Babub, B.S., 2015, "Characterization of Chemical Reaction on Heat Transfer Through the Nanofluid," *Procedia Materials Science*, **10**, 10-18.  
<https://doi.org/10.1016/j.mspro.2015.06.018>

Sandeep, N., and Sulochana, C., 2016, "Momentum and Heat Transfer Behaviour of Jeffrey, Maxwell and Oldroyd-B Nanofluids past a Stretching Surface with Non-uniform Heat Source/Sink," *Ain Shams Engineering Journal*, **xxx**, xxx-xxx.  
<https://doi.org/10.1016/j.asej.2016.02.008>

Saadatfara, B., Fakhraia, R. and Franssona, T., 2015, "Conceptual Modeling of Nanofluid ORC for Solar Thermal Polygeneration," *Energy Procedia*, **57**, 2696-2705.  
<https://doi.org/10.1016/j.egypro.2014.10.301>

Shrama, P. R. and Singh, G., 2010, "Steady MHD Natural Convection

Flow with Variable Electrical Conductivity and Heat Generation along an Isothermal Vertical Plate" *Tamkang Journal of Science and Engineering*, **13**(3), 235-242.  
[www2.tku.edu.tw/~tkjse/13-3/02-M9707.pdf](http://www2.tku.edu.tw/~tkjse/13-3/02-M9707.pdf)

Afikuzzaman, M., Ferdows, M., and Alam, M. M., 2015, "Unsteady MHD Casson Fluid Flow through a Parallel Plate with Hall Current," *Procedia Engineering*, **105**, 287-293.  
<https://doi.org/10.1016/j.proeng.2015.05.111>

Afikuzzaman, M., and Alam, M. M., 2016, "MHD Casson Fluid Flow through a Parallel Plate," *Thammasat International Journal of Science and Technology*, **21**(1).  
<https://tci-thaijo.org/index.php/SciTechAsia/52122>

Wahiduzzaman, M., Islam, M. T., Sultana, P., and Afikuzzaman, M., 2014, "MHD Couette Flow of a Casson Fluid between Parallel Porous Plates," *Progress in Nonlinear Dynamics and Chaos*, **2** (2), 51-60.  
<http://www.researchmathsci.org/PINDACart/PINDAC-v2n2-6.pdf>

Biswas, R. and Ahmmed, S. F., 2018, "Effects of Hall Current and Chemical Reaction on Magnetohydrodynamics Unsteady Heat and Mass Transfer of Casson Nanofluid Flow through a Vertical Plate", *Journal of Heat Transfer*, **140**(9).  
<http://cps.kwglobal.com/MIS/AuthorProofLogin.aspx?pwd=2044225d84e5&CA=AS>

Ahmmed, S. F., Biswas, R. and Afikuzzaman, M., 2018, "Unsteady Magnetohydrodynamic Free Convection Flow of Nanofluid Through an Exponentially Accelerated Inclined Plate Embedded in a Porous Medium with Variable Thermal Conductivity in the Presence of Radiation", *Journal of Nanofluids*, **7**, 891-901.  
<https://doi.org/10.1166/jon.2018.1520>

Kataria, H. R. and Patel, H. R., 2018, "Effect of Thermo-Diffusion and Parabolic Motion on MHD Second Grade Fluid Flow with Ramped Wall Temperature and Ramped Surface Concentration", *Alexandria Engineering Journal*, **57**, 73-85.  
<https://doi.org/10.1016/j.aej.2016.11.014>

Kataria, H. R. and Patel, H. R., 2016, "Soret and Heat Generation Effects on MHD Casson Fluid Flow past an Oscillating Vertical Plate Embedded through Porous Medium", *Alexandria Engineering Journal*, **55**, 2125-2137.  
<https://doi.org/10.1016/j.aej.2016.06.024>

Kataria, H. R. and Patel, H. R., 2016, "Radiation and Chemical Reaction Effects on MHD Casson Fluid Flow past an Oscillating Vertical Plate Embedded in Porous Medium", *Alexandria Engineering Journal*, **55**, 583-595.  
<https://doi.org/10.1016/j.aej.2016.01.019>

Sheikholeslami, M., Kataria, H. R., and Akhil, S. M., 2017, "Radiation Effects on Heat Transfer of Three Dimensional Nanofluid Flow Considering Thermal Interfacial Resistance and Micro Mixing in Suspensions", *Chinese Journal of Physics*, **55**, 2254-2272.  
<https://doi.org/10.1016/j.cjph.2017.09.010>

Sheikholeslami, M., Kataria, H. R., and Akhil, S. M., 2018, "Effect of Thermal Diffusion and Heat-Generation on MHD Nanofluid Flow past an Oscillating Vertical Plate through Porous Medium", *Journal of Molecular Liquids*, **257**, 12-25.  
<https://doi.org/10.1016/j.molliq.2018.02.079>